

## Acoustic Agitation for Enhanced Development of LIGA PMMA Resists

§R. H. Nilson and S. K. Griffiths

Sandia National Laboratories, Livermore, California 94551-0969

### ABSTRACT

The development of exposed PMMA resists for the LIGA process is difficult and time-consuming when the resist thickness is large (~1 mm) and feature aspect ratios exceed about four. This is due mainly to limitations on the development rate imposed by the diffusive transport of PMMA fragments away from the dissolution surface. Development rates under these conditions can be enhanced significantly by high-frequency acoustic agitation. To study this enhancement, analytical solutions describing the periodic flow field are used to evaluate the time-mean Reynolds stresses that drive streaming fluid motion. The resulting steady flow and transport rates within a feature are then computed by solving the Navier-Stokes and species transport equations. For typical acoustic frequencies and power levels of 1 MHz and 6 w/cm<sup>2</sup> the streaming flow within the feature is toroidal, with inflow along the feature walls at speeds approaching 25 μm/s, coupled with a slower outflow along the feature center. The computed increase in transport, relative to diffusion, is typically on the order of 4 to 6 for feature aspect ratios ranging from 3 to 10 and for polymer fragment diffusivities on the order of 10<sup>-11</sup> m<sup>2</sup>/s, provided that the feature width is greater than about 10 microns. In smaller features, the streaming speed may be suppressed by overlapping viscous boundary layers on opposing feature walls. Higher frequencies help reduce the boundary layer thickness but may lead to less efficient multi-cellular flow patterns when the acoustic wavelength (~1 mm at 1MHz) is less than the feature depth.

**Keywords:** LIGA, development, transport, ultrasonic, sonic, agitation, acoustic, streaming, microstructures

### 1. INTRODUCTION

LIGA is a multistep process used to manufacture high-resolution, high aspect-ratio microdevices having micron to millimeter features.<sup>1,2</sup> The acronym is derived from the German words for lithography, electroforming and molding. In LIGA, a high-energy x-ray source is used to expose a thick photoresist, typically PMMA, through a lithographically produced mask. The exposed material is then removed by chemical dissolution in a development bath. This development process yields a nonconducting mold having cavities that are subsequently filled by means of electrodeposition. The resulting metal parts may be the final product or may be used as injection or embossing molds for mass production.

Both PMMA resist development and electrodeposition for LIGA suffer from several practical problems when feature aspect ratios are large. For development, these include incomplete dissolution of the exposed PMMA, undercutting of the interface between the PMMA and its conductive substrate, and sidewall development into low-dose regions within the masked area. For electrodeposition, these problems may include poor metal morphology and highly nonuniform deposition rates in features of widely differing size. In both processes, the time required for completion may be lengthy, ranging up to several hours for development and even days for electrodeposition.

Many of these problems arise from a common origin of transport limitations between the top surface of the PMMA mold and the dissolution or deposition interface. In development, dissolved polymer fragments must be transported from the dissolution surface to the bath. Similarly, metal ions in electrodeposition must be transported from the bath to the plating surface. In deep narrow features, both of these processes are often diffusion limited because the fluid within the feature is usually nearly stagnant.

Stirring or pumping of the bath fluid is helpful in maintaining bath conditions adjacent to the mold top. However, even a very strong flow across the top is not effective in providing increased transport into features having aspect ratios greater than

---

§Correspondence – Email: [rhnilso@sandia.gov](mailto:rhnilso@sandia.gov); Telephone: (925) 294-3571  
Sandia LIGA Web Page: <http://daytona.ca.sandia.gov/LIGA/>

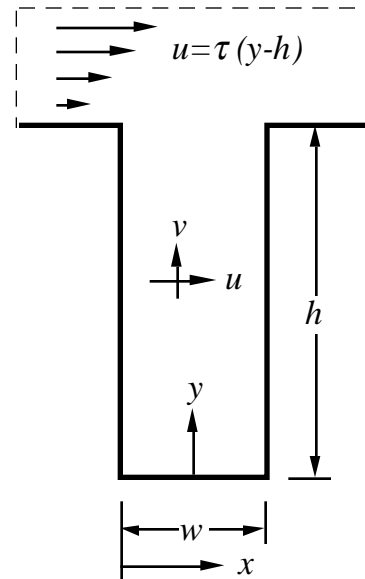
about two.<sup>3</sup> This is because the convective cell that circulates the fluid in the top of each feature penetrates only one feature width below the mold top. Additional counter-rotating convective cells are formed deeper within high aspect-ratio features, but the circulation speeds in successive cells decrease by nearly two orders of magnitude.<sup>4</sup> Thus, high aspect-ratio features are essentially stagnant over most of their height, while low aspect-ratio features are well stirred throughout. This disparity leads to large nonuniformities in development and deposition rates when feature depths are large.

Acoustic agitation offers a promising means for enhancing transport rates within high aspect-ratio features. A number of researchers have demonstrated experimentally that LIGA development rates can be increased several fold by performing the process in acoustic baths like those used for cleaning semiconductor wafers.<sup>3,5,6,7</sup> In most of these studies it is suggested that the collapse of acoustically generated bubbles is responsible for increased development rates. Although the exact mechanism is uncertain, bubble collapse is thought to generate very large local temperatures that increase surface reaction rates.<sup>8</sup> In addition, pressure forces produced by collapsing bubbles may help to dislodge particles or adsorbed species that are loosely bound to surfaces. Both of these mechanisms may be operative in LIGA development and may explain increased development rates in shallow features having small to moderate aspect ratios. However, the fact that LIGA development rates decrease substantially with increasing feature depth, even under acoustic agitation, strongly suggests that development rates of high aspect-ratio features are limited by transport within features, not by surface reaction rates. It follows that the principal benefit of acoustic agitation is improved feature-scale transport.

The thesis of this paper is that high-frequency acoustic agitation enhances development by producing a steady streaming flow that circulates most of the fluid within features, substantially increasing species transport. Although the fluid dynamics of acoustic streaming has been studied extensively<sup>9,10,11</sup>, there have been no previous studies of the induced species transport in cavities and recesses typical of LIGA features. To better understand this process, analytical and numerical methods are used to solve the equations governing flow and species transport within trench-like features. The sound field is described by superposition of exact solutions derived by Rayleigh<sup>9</sup> and Nyborg.<sup>10</sup> The time-mean Reynolds stresses computed from these harmonic solutions are then used as the driving forces in a numerical solution of the Navier-Stokes equations. The resulting steady acoustic streaming flow is finally used to compute the transport of a representative chemical species by diffusion and advection. Solutions are presented for parameters typical of LIGA development and deposition processes. These results are also compared with those of previous experimental studies.

**Figure 1.** Schematic of a trench-like LIGA feature. In development, dissolved polymer fragments are transported from the dissolution front to the mold top. Conversely, in electrodeposition, metal ions are transported from the mold top to the deposition surface at the feature bottom. Although the feature height varies during development and deposition, the motion of the feature bottom is sufficiently slow that flow and transport processes may be presumed quasi-steady for a given feature height.

Fluid motion within the feature is driven mainly by harmonic pressure variations at the feature mouth. The fluid velocity across the mold top, shown by arrows, circulates the fluid in the feature top, but only to a depth equal to about one feature width. Thus, the fluid deep within high aspect-ratio features can only be circulated by acoustic agitation.



## 2. GOVERNING EQUATIONS

To model the effects of acoustic agitation in LIGA molds we consider the simplified geometry of a single trench-like feature as shown in Figure 1. In the region far above the mold,  $y \gg h$ , the bath is presumed to be well mixed and to have a negligible concentration of dissolved polymer fragments or a uniform concentration of metal ions. Since the frequency,  $f$ , and intensity,  $I$ , of the sound field are known for commercial acoustic baths, these conditions are used to characterize the acoustic motion at the mouth of the feature. The effects of bath stirring are modeled by prescribing a steady uniform flow

from left to right above the mold. This uniform external flow produces a linear gradient of the fluid speed in a boundary layer just above the mold top. The resulting shear force is transmitted to the fluid at the top of the feature, driving motion within the feature. However, as noted earlier, the effects of this forced convection are negligible when the aspect ratio is large.

The fluid velocity field within the feature is governed by the Navier-Stokes equations. A direct numerical solution of these equations is possible but somewhat impractical because of the large difference in the time scales of acoustic agitation and chemical development. Since the period of a typical 1 MHz acoustic wave is only one microsecond, billions of numerical time steps would be needed to span even a few minutes of development time. To deal with this disparity we will utilize a method of successive approximations that has been used previously in solving problems of this general class.<sup>9,10,11</sup> The pressure,  $p$ , density,  $\rho$ , and velocity  $\mathbf{u}=\mathbf{u}_i+\mathbf{v}_j$  are each written as an infinite series.

$$\mathbf{u} = \mathbf{u}_a + \mathbf{u}_s + \dots \quad p = p_0 + p_a + p_s + \dots \quad \rho = \rho_0 + \rho_a + \rho_s + \dots \quad (1)$$

The ambient values of pressure and density,  $p_0$  and  $\rho_0$ , are taken as constant and uniform. The acoustic terms, subscripted  $a$ , are assumed to be harmonic functions of time but may vary arbitrarily with position. The steady acoustic streaming terms, subscripted  $s$ , are time invariant but again are free to vary spatially. These series expansions are substituted into the Navier-Stokes equations and terms of like order are equated to one another. The first order harmonic terms and their products with  $p_0$  and  $\rho_0$  yield the linearized acoustic equations.<sup>9,10,12</sup>

$$\frac{\partial \rho_a}{\partial t} + \rho_0 \nabla \cdot \mathbf{u}_a = 0 \quad \rho_0 \frac{\partial \mathbf{u}_a}{\partial t} = -\nabla p_a + \mu \nabla^2 \mathbf{u}_a + \left(\mu_b + \frac{1}{3}\mu\right) \nabla (\nabla \cdot \mathbf{u}_a) \quad (2)$$

Here,  $\mu$  and  $\mu_b$  are the shear and bulk viscosities. The acoustic pressure and density variations are generally related by the equation of state,  $p_a=c_0^2\rho_a$ , in which  $c_0$  is the speed of sound. These equations can be solved by superposing solutions derived by Rayleigh for traveling waves in tubes and channels of infinite length, as explained later. The equations governing the acoustic streaming flow are deduced by taking the time average of the series expansion of the Navier-Stokes equations. The averaging process eliminates all of the simple harmonic terms that appeared in the preceding linear acoustic equations but leaves the steady flow quantities subscripted  $s$  below as well as the time averaged products of harmonic functions that are gathered into  $\mathbf{F}$ .<sup>10</sup>

$$\nabla \cdot \mathbf{u}_s = 0 \quad \nabla p_s - \mu \nabla^2 \mathbf{u}_s = \mathbf{F} \quad \mathbf{F} = -\rho_0 \left\langle \left( \mathbf{u}_a \cdot \nabla \right) \mathbf{u}_a + \mathbf{u}_a \left( \nabla \cdot \mathbf{u}_a \right) \right\rangle \quad (3)$$

The steady streaming motion is driven by an apparent body force,  $\mathbf{F}$ , arising from the Reynolds stresses produced by the harmonic motion. Note that the time averaging brackets,  $\langle \rangle$ , that enclose the Reynolds stresses have been dropped from the time invariant quantities,  $\mathbf{u}_s$  and  $p_s$ , because they are redundant. Although it is essential that compressibility be retained in the preceding acoustic equations, the streaming flow may be assumed incompressible. In addition, the inertial terms have been deleted from Eq. (3b) because the Reynolds number of the acoustic streaming flow is generally far less than unity. Note, however, that the streaming motion is actually driven by the inertial forces of the acoustic motion. The solution procedure is as follows: solve Eqs. (2) analytically for the harmonic velocity field; evaluate the Reynolds stresses that comprise  $\mathbf{F}$ ; numerically solve Eqs. (3) for the steady streaming flow. The steady velocity field is then used in numerically solving the following conservation equation describing steady diffusive and advective transport of a single chemical species.

$$\mathbf{u}_s \cdot \nabla C = D \nabla^2 C \quad (4)$$

Here,  $C$  is the molar density of the conserved species that may be either the polymer fragment concentration in development or the metal ion concentration in electroplating;  $D$  is the diffusivity of that species.

### 3. HARMONIC VELOCITY FIELD

High frequency pressure variations at the feature mouth drive the acoustic motion within the feature. Rayleigh<sup>9</sup> derived traveling wave solutions that satisfy the two-dimensional cartesian form of the acoustic wave equations (2) for a channel bounded by infinite parallel planes, subject to nonslip and impermeable boundary conditions on the bounding walls. These solutions can be applied directly to the trench-like feature geometry of Figure 1. The  $u$  and  $v$  velocity components of the Rayleigh solution are each proportional to the nominal acoustic velocity  $u_{a0}$  which is matched to the sound intensity,  $I$ , in the bath at the feature mouth. The velocity component along the feature axis is generally orders of magnitude greater than

the transverse component. Because of the noslip condition, thin viscous boundary layers develop interior to the feature along the feature side walls. The viscous boundary layer thickness,  $\delta$ , is nearly uniform along the feature height. The simple formulas given below can be used to calculate  $u_{a0}$ ,  $\delta$  and the acoustic wave length,  $\lambda$ .

$$u_{a0} = \sqrt{\frac{I}{\rho c}} \approx 0.2 \text{ m/s} \quad \lambda = \frac{c}{f} \approx 1.5 \text{ mm} \quad \delta = \sqrt{\frac{2\mu}{\omega\rho}} \approx 0.6 \text{ }\mu\text{m} \quad (5)$$

The approximate values above are based on a frequency  $f=\omega/2\pi=1\text{MHz}$  and sound intensity  $I=6 \text{ w/cm}^2$ , typical of commercial wafer cleaning baths and fluid properties like those of water:  $\rho=1000 \text{ kg/m}^3$ ;  $c=1500 \text{ m/s}$ ; and  $\mu=10^{-3}\text{Ns/m}^2$ . In addition to the scaling constant,  $u_{a0}$ , the Rayleigh solution contains three dimensionless parameters: the normalized wave length,  $\lambda/w$ ; the aspect ratio,  $h/w$ ; and normalized thickness of the viscous boundary layers,  $\delta/w$ . For given choices of these parameters, there are two solutions representing waves traveling in opposite directions along the feature. To obtain the full solution, we must generally superpose the downward traveling wave with its upward traveling reflection off the lower surface.

The reflected wave will strongly influence the velocity field when the feature bottom is highly reflective. This is certainly the case in electroplating because the metal plating surface at the mold bottom has an acoustic impedance much greater than that of the electrolyte. In this instance, the combination of the primary and reflected waves produces a standing wave having increased fluid motion in some locations and reduced motion in others. The resulting acoustic streaming patterns are also strongly affected and become cellular in character rather than unidirectional.<sup>9</sup> In LIGA development, however, the polymer surface at the mold bottom has a density and wave speed that typically exceed those of the developer fluid by only about 20% and a factor of two to three, respectively. Under these conditions the impedance mismatch is less severe, and the amplitude of the reflected wave is only 20% to 30% as great as that of the wave incident in the interface. For this reason, and for the sake of simplicity, the reflected wave will not be included in the example calculations presented here.

Figure 2 shows the computed amplitude of the longitudinal velocity,  $v_a$ , along the feature as a function of transverse position for several choices of the normalized boundary layer thickness,  $\delta/w$ . The solid lines represent the Rayleigh solution explained above while the dotted lines represent the following approximate solution derived by Nyborg in the limit where the viscous boundary layers are thin compared to the feature width.<sup>10</sup>

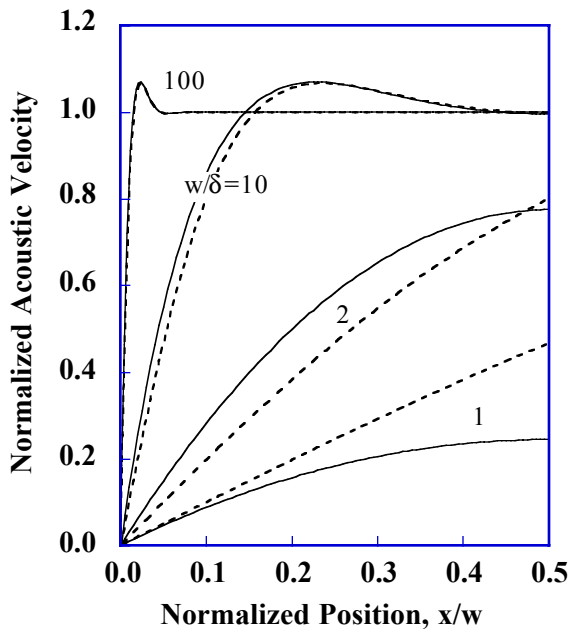


**Figure 2.** Normalized acoustic velocity,  $v_a/u_{a0}$ , at feature top versus normalized transverse position. Feature wall is at left; feature center is at right of plot. Solid lines are Rayleigh solution; dotted lines are approximation of Eq. (6a).

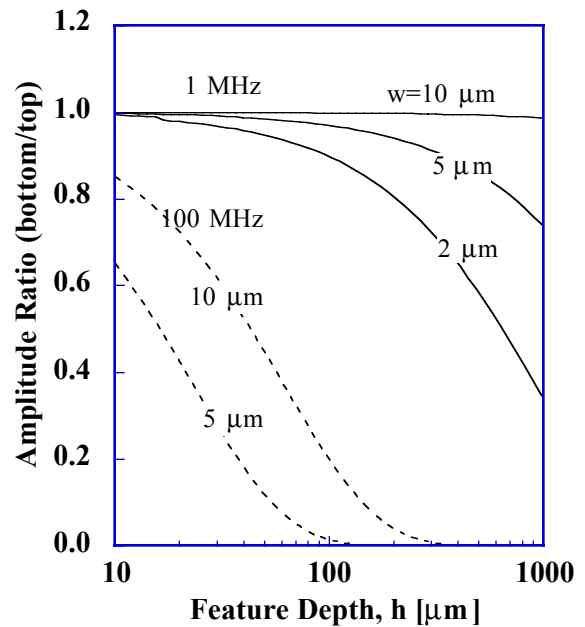


**Figure 3.** Attenuation of acoustic velocity along feature versus feature depth. At 1 MHz attenuation is unimportant for millimeter-depth LIGA features provided that feature width is greater than about 10  $\mu\text{m}$ .

$$v_a \approx u_{a0} \left( 1 - e^{-\frac{(1+j)x}{\delta}} \right) e^{\pm \left( \alpha + j \frac{2\pi}{\lambda} \right) y} e^{j\omega t} \quad \text{and} \quad u_a \approx -v_a 2\pi \frac{\delta}{\lambda} \left( \frac{j}{1+j} \right) \quad (6)$$

Here,  $j = (-1)^{1/2}$  and the real part of each function is implied. As seen in Figure 2, the approximate solution provides a very good estimate, provided that  $w/\delta > 10$ . For typical LIGA parameters  $\delta < 1 \mu\text{m}$ , so the approximate solution should remain valid for features having widths of 10 microns or more. For features much smaller than this the acoustic velocity within the feature will be severely diminished, as seen in Figure 2. These velocity profiles are applicable at the top of the feature.

In addition to the viscous damping of the fluid motion at the top of the feature, as seen in Figure 2, there is also attenuation of the amplitude between the top and bottom of the feature. This is not fully accounted for in the approximation of Eq. (6) as it is derived in the limit of infinite feature width. However, the more complete Rayleigh solution indicates that for attenuation of 30% or less, the pressure and velocity amplitudes decay nearly exponentially such that the ratio of bottom to top amplitudes is  $\exp(-h\delta/\lambda w)$ . Figure 3 illustrates the attenuation computed from the full solution. It is seen that wave attenuation is insignificant at 1MHz for millimeter-depth features provided that the feature width is greater than 10 microns, so this effect is usually negligible in LIGA. Note that the attenuation increases at higher frequencies because of the reduced wavelength but, again, this is generally not of concern in LIGA.

#### 4. ACOUSTIC STREAMING IN HIGH ASPECT-RATIO FEATURES

The acoustic streaming motion in deep features having weakly reflective bottoms can be well approximated using an approach suggested by Nyborg.<sup>10</sup> Over most of the height of a tall slender feature, the streaming velocity is nearly vertical, so the transverse velocity component can be neglected to obtain the following simplification of Eqs. (3).

$$\int_0^w v_s dx = 0 \quad \text{and} \quad \mu \frac{\partial^2 v_s}{\partial x^2} = \frac{\partial p_s}{\partial y} - F_y \quad (7)$$

The driving Reynolds stresses  $F_y$  acting in the vertical direction are evaluated by substituting the preceding asymptotic solution of Eqs. (6) into the definition of  $F$  given in Eq. (3c). The resulting velocity profile,  $v_s(x)$ , is then determined by analytically integrating Eq. (7a) across the feature subject to nonslip conditions at the feature walls. In doing this, the

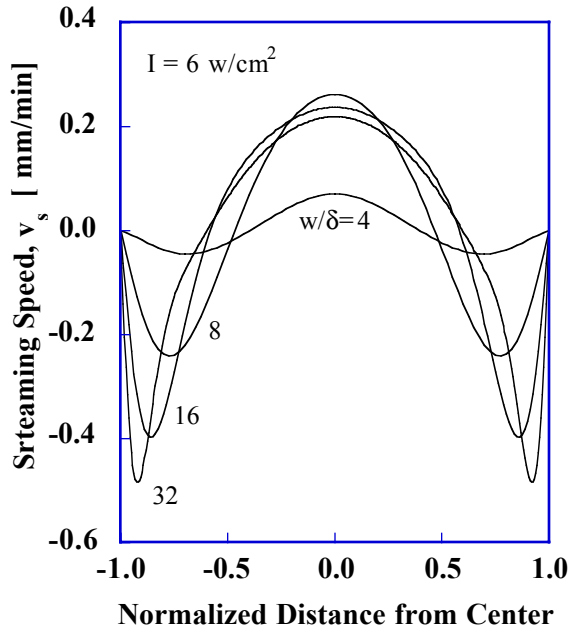


**Figure 4.** Acoustic streaming velocity versus normalized distance from feature center. Viscous forces reduce vertical fluid speed in narrow features.

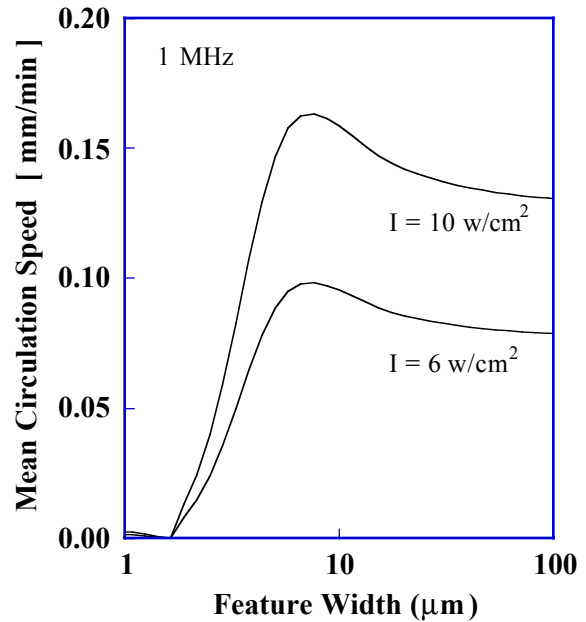


**Figure 5.** Mean circulation speed versus feature width. Mean speed is computed by averaging vertical velocity profile across upflow or downflow regions.

vertical pressure gradient is assumed to be constant and is determined by enforcing the above integral constraint that the net vertical flow through any horizontal cross section must be identically zero. These solutions are suggested but not presented or displayed by Nyborg and so are included here in Figure 4.

The velocity profiles in Figure 4 illustrate typical streaming flow conditions along the central section of a deep feature. The downward flow along the feature walls is driven by large Reynolds stress gradients in the acoustic boundary layers adjacent to the walls. The upflow in the center is simply a consequence of continuity. As the acoustic boundary layers grow thicker, the streaming motion is suppressed quite like the acoustic motion illustrated in Figure 2. But the streaming remains relatively strong for features more than ten-fold wider than the micron scale of the acoustic boundary layers. The same behavior is illustrated in Figure 5 where the mean circulation speed falls off sharply for feature widths less than a few microns.

The nominal speed of acoustic streaming adjacent to a solid surface can be estimated from the following formula

$$u_{s0} \equiv \frac{u_{a0}^2}{c_0} \approx 25 \mu\text{m/s} \quad (8)$$

in which the numerical values are again for an acoustic intensity of  $I=6 \text{ w/cm}^2$  and a fluid like water with a density of  $1000 \text{ kg/m}^3$ , and sound speed,  $c_0$ , of  $1500 \text{ m/s}$ . Note that the nominal streaming speed is independent of viscosity; this is because the driving force  $F$  and the resisting shear forces are both proportional to the viscosity. In wide features a maximum speed of about  $u_{s0}/4$  is reached at the edge of the viscous boundary layer<sup>10</sup>, just a micron or so from the feature wall. However, as the feature width grows narrower, viscous forces increase and the maximum velocity is reduced. Although the velocity profiles of Figure 4 can be deduced analytically, we have found it expedient to use numerical methods to compute the resulting species transport and enhancement of LIGA development and electrodeposition rates.

## 5. NUMERICAL MODELING OF SPECIES TRANSPORT BY ACOUSTIC STREAMING

Numerical methods are used to investigate the transport of polymer fragments or metal ions induced by acoustic streaming in LIGA features. The Navier-Stokes equations (3) governing the streaming motion were rewritten in terms of the stream function and vorticity, as appropriate for steady incompressible flows. These equations and the species transport equation (4) were discretized using second-order finite differences to obtain a system of algebraic equations for nodal point values of the stream function, vorticity, velocity components, and species concentration.<sup>4</sup> These equations were solved iteratively on a rectangular mesh covering the T-shaped domain shown in Figure 1. In each solution, iterations were continued until the solution was fully converged on successively finer meshes containing 21, 41, and 81 grid points across the feature width. Since the rectangular grid was equally spaced in both directions and in all locations, the number of grid lines in the vertical direction was, for example, 801 for a feature aspect ratio of 10.

Although the numerical model had been previously tested for a variety of flow conditions, additional tests were performed to verify that acoustic streaming was correctly computed. To this end, numerical results were compared to the analytical velocity profiles shown previously in Figure 4. It was found that calculations performed with 81 grid points across the feature were in good agreement with the analytical results provided that the relative thickness of the viscous boundary layer,  $\delta/w$ , was no less than  $\sim 0.05$ . Since the boundary layers are often much thinner than this in LIGA applications, calculations were also performed by applying a slip velocity boundary condition along the vertical walls with a speed of  $u_{s0}/4$ , as appropriate for boundary layers much thinner than the feature width. The velocity profiles computed with this approach were in very good agreement with the exact asymptotic solutions, even for sparse grid spacing. In addition, it was found that species transport computed with the slip velocity approach differed little from that driven by explicit use of the Reynolds stresses comprising  $F$  in Eq. (3c). Thus, since numerical convergence is greatly improved by application of slip boundary conditions, this method is used in most of the results presented here. However, it is emphasized that this approach can only be used under the restriction that  $w/\delta \gg 1$ .

To reduce the number of solution parameters, the position coordinates were scaled by the feature width,  $w$ , the velocity components by  $D/w$ , and the stream function and vorticity by  $D$  and  $D/w^2$ , where  $D$  is diffusivity of the transported species. The species concentration is scaled by its overall variation, such that the normalized concentrations in the bath and feature bottom are simply zero and unity. The resulting equations contain three dimensionless parameters, the Peclet Number, aspect ratio, and normalized thickness of the acoustic boundary layer.

$$Pe_w = \frac{u_{s0} w}{D} \quad A = \frac{h}{w} \quad \delta^* = \frac{\delta}{w} \quad (9)$$

The Peclet number,  $Pe_w$ , indicates the relative strength of convective transport by acoustic streaming compared to transport by diffusion; it is proportional to the nominal streaming speed,  $u_{s0}$ , explained previously. When slip velocities are applied to the feature walls the normalized slip speed is simply  $Pe_w/4$ . When Reynolds stress are used to drive the motion, solutions also depend on  $\delta/w$ . In either case, the normalized fluid speed across the top of the T-shaped domain of Figure 1 is taken as equal to the nominal streaming speed within the feature, a very slow speed relative to the bath scale. In the absence of additional stirring, a streaming motion of this magnitude would probably occur along the mold face and, as noted earlier, is of little importance for features having aspect ratios greater than two or three.

The most important result of the numerical calculations is the Sherwood Number,  $Sh$ , representing the ratio of the computed vertical species transport to that which would have occurred by diffusion alone. Under quasisteady conditions,  $Sh$  is the same at all elevations within the feature. It is most conveniently calculated at the feature bottom where the vertical velocity is zero and the transport occurs locally by diffusion alone.

$$Sh = \left( \frac{h}{D \Delta C} \right) \frac{1}{w} \int_0^w D \frac{\partial C}{\partial y} dx = A \int_0^1 \frac{\partial C^*}{\partial y^*} dx^* \quad (10)$$

In the absence of fluid motion, the normalized gradient at the bottom is  $1/A$  and  $Sh$  is unity. In the presence of acoustic streaming, advective transport sweeps fresh developer across the feature bottom, producing a steeper boundary-layer gradient.

Figures 6 and 7 illustrate computed flow and transport within features having an aspect ratio of 4 for two different choices of the Peclet number. Streamlines are shown on the left side of each figure. Isopleths, or lines of constant species concentration, are shown on the right side. The flow within the feature is torroidal with downflow along the walls and upflow in the center. The flow turns at the top and bottom over regions having a vertical extent of about one half feature width. Some of the flow coming in from the left along the mold top descends into the feature, returns up the center and rejoins the external flow. As noted previously, the overall transport is not strongly influenced by the flow over the feature top. The flow along the midsection of the feature is nearly identical to the analytical solutions shown earlier in Figure 4. Note the very strong similarity of the streamlines in Figures 6 and 7. This similitude holds even though the calculation of Figure 6 was driven by Reynolds stress in the boundary layers, whereas the flow in Figure 7 is driven by a slip velocity at the wall. Because of this difference, the streamlines of Figure 7 are more closely spaced near the walls, indicating higher speeds adjacent to the walls. Other features of these plots are discussed in the extended captions at the side of each.

**Figure 6.** Computed streamlines (left) and concentration isopleths (right) for a Peclet number of  $Pe_w=125$  and an aspect ratio of  $A=h/w=4$ . These conditions correspond to  $I=10$  watts/cm<sup>2</sup>,  $w=30$   $\mu$ m,  $h=120$   $\mu$ m, and  $D=10^{-11}$  m<sup>2</sup>/s. Relative thickness of acoustic boundary layer is taken as  $\delta/w=1/16$ , somewhat thicker than typical of LIGA.

Flow along the midsection does not vary with elevation and is equivalent to that shown in Figure 4. With increasing aspect ratio, the flow along the midsection remains the same but is extended over a longer midsection; turning regions at the ends are not affected.

Isopleths are bent downward by descending flow adjacent to feature walls. Upward flow in center is also apparent. Close spacing of isopleths near feature bottom indicates large diffusion flux at lower surface. The Sherwood number for these conditions is about 3.5, indicating a three- to four-fold enhancement of species transport and development rate.

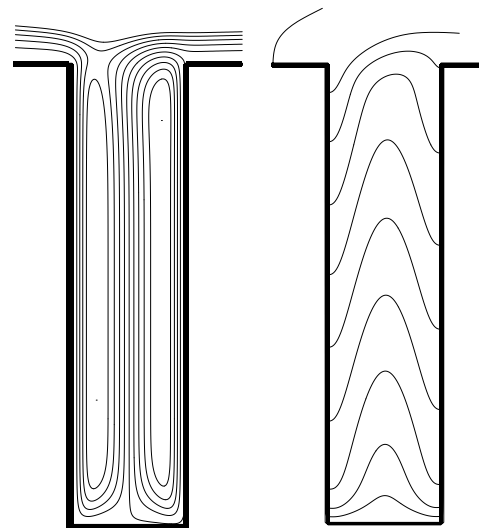


**Figure 7.** Computed streamlines (left) and isopleths (right) for a Peclet number of 500 and an aspect ratio of  $A=h/w=4$ . Compared to Figure 6, these conditions correspond to a four-fold increase in bath intensity or feature width or a four-fold decrease in species diffusivity.

Streaming flow field is driven by a slip velocity at the wall, rather than including acoustic Reynolds stresses in Navier-Stokes equations, as done in Figure 6. Streamline pattern is hardly altered by this or the increase in Peclet number; flow structure is dependent only on viscous boundary layer thickness and aspect ratio.

Isopleths are strongly effected by four-fold increase of Peclet number. Stronger downflow sweeps isopleths steeply downward. Very large concentration gradients at feature bottom indicate high species fluxes. Computed Sherwood number of about 22 indicates a similar enhancement of transport and development rate compared to diffusion-limited rate.

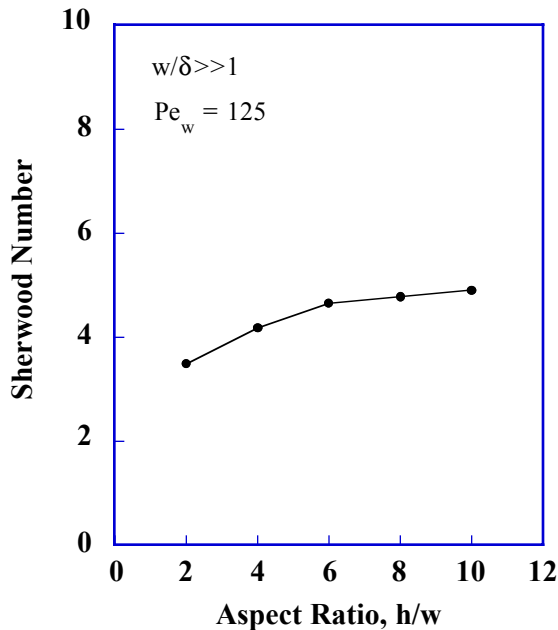
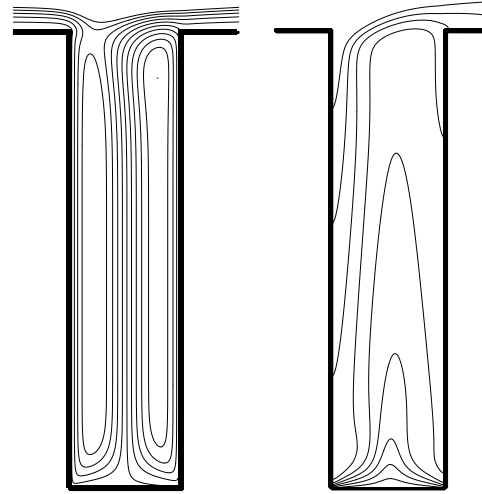


**Figure 8.** Variation of Sherwood number with aspect ratio. Sherwood number indicates enhancement of transport rate and, hence, development rate relative to diffusion. Symbols represent calculations, not experimental data.

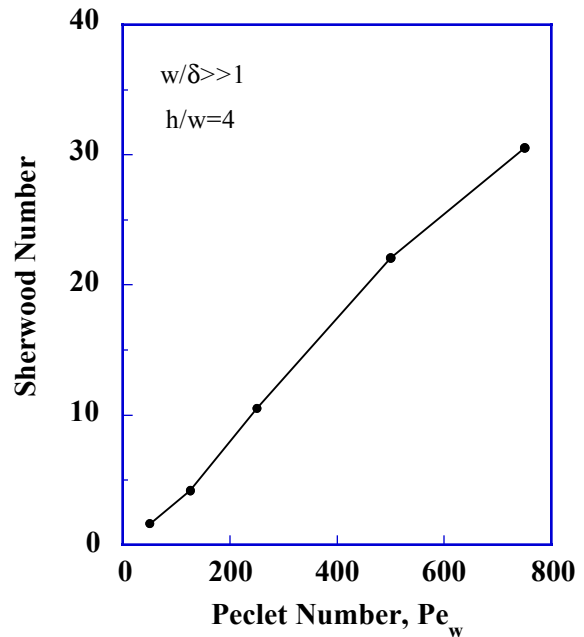


**Figure 9.** Variation of Sherwood number with Peclet number. Higher  $Pe$  corresponds to a higher streaming speed, larger feature width and depth, or lower diffusivity. Symbols represent calculations, not experimental data.

Figure 8 shows that the computed Sherwood number,  $Sh$ , increases with aspect ratio up to an aspect ratio of about 10. Beyond that point, it appears that  $Sh$  reaches an asymptotic value of about 4.5 for a Peclet number of 125. This behavior is probably beneficial to the uniformity of LIGA development rates in features of differing widths because acoustic streaming provides the greatest benefit in high aspect-ratio features that receive the least benefit from bath stirring. Thus, these two factors should be somewhat offsetting when both methods are used to increase development rates. Since the Peclet number based on the feature width is fixed in Figure 8, this sequence of calculations describes the variation of  $Sh$  in a feature of fixed width and varying depth. Thus, the results imply that the benefit of acoustic streaming does not diminish with increasing feature depth.

Figure 9 indicates that the Sherwood number and development rate increase roughly linearly with Peclet number over the range investigated. Thus, for a fixed geometry, a doubling of bath intensity and hence streaming speed (since  $u_{s0} \sim I$  by Eqs. (5) and (7)) will produce a doubling of the development rate. If the bath intensity is held fixed, Figure 9 indicates that a doubling of feature width (and height as well, with  $A$  held fixed) will also double the development rate. At very low Peclet numbers, the Sherwood number approaches unity. At high Peclet numbers, the rate of increase in Sherwood number appears to be decreasing. Work is in progress to analytically explore the regimes of large Peclet number and large aspect ratio, as calculations become progressively time consuming in these extremes.

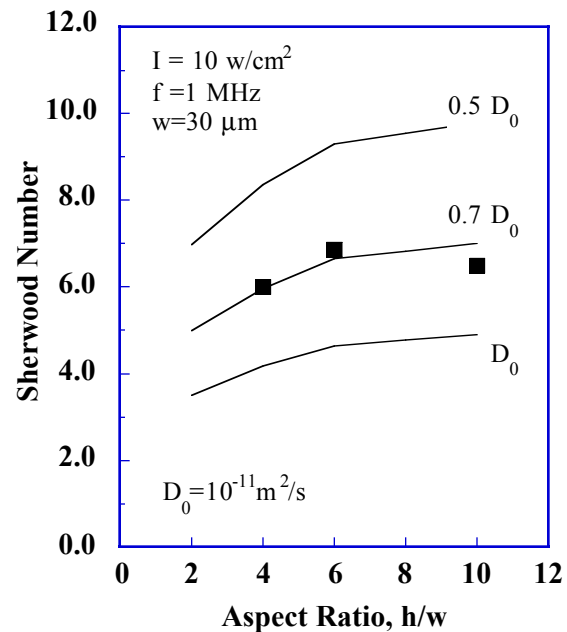
It is concluded from Figure 9 that acoustic agitation will not provide significant benefits in LIGA electrodeposition. This is because Peclet numbers based on typical metal ion diffusivities of  $10^{-9} \text{ m}^2/\text{s}$  will be no greater than about 10 for typical bath intensities and feature widths of  $100 \text{ }\mu\text{m}$  or less. As seen in Figure 9, the corresponding Sherwood number is not much greater than unity. In development, however, polymer fragment diffusivities are orders of magnitude smaller, thereby increasing the relative importance of acoustic agitation, as explained in the next section.

## 6. COMPARISON WITH EXPERIMENTAL DATA

To our knowledge, the data most relevant to the present study is that of Zanghellini et al.<sup>3</sup> In Figure 3 of that paper the authors present measured development rates for  $30 \text{ }\mu\text{m}$  features developed with and without acoustic agitation. By taking the ratio of these two measured rates we obtain a relatively direct measure of the Sherwood number representing the ratio of transport rates with and without agitation. In doing this we use as our denominator the measured development rates they characterize as dip developed with no bath stirring. These conditions should be equivalent to diffusion-limited development. The three data points shown in Figure 10, for aspect ratios from 4 to 10, cover the full range for which the authors reported data for both experiments. It is seen that the data (symbols) and calculations (lines) both suggest that the Sherwood number is relatively constant over the range of the data. The variation in the data shown could easily result from inaccuracy in our reading of the plotted experimental data.

**Figure 10.** Comparison of numerical calculations (solid lines) with enhancement of development rates (symbols) observed by Zanghellini et al.<sup>3</sup> Bath intensity, frequency, and feature widths and depths used in the calculations are the same as reported experimental conditions. The lowest line corresponding to  $D=D_0=10^{-11} \text{ m}^2/\text{s}$  is identical to that shown in Figure 8 for  $Pe_w=125$ . Experimental Sherwood number is obtained by taking ratio of observed development rates, with and without agitation, for features of identical width and depth.

Observed enhancement of development rate is in best agreement with calculations based on a fragment diffusivity of  $0.7 \times 10^{-11} \text{ m}^2/\text{s}$ , a reasonable value for large polymer fragments. Variation of Sherwood number, or equivalently enhancement, with aspect ratio is also consistent with that observed experimentally.



The measurements shown by bold symbols in Figure 10 are compared with theoretical calculations for three different choices of the unknown polymer fragment diffusivity. The other parameters used in the calculations are the experimental intensity and frequency of the bath. These are the only important parameters, since at 1 MHz the acoustic boundary layers are thin compared to the feature width, even for development fluids ten-fold more viscous than water. The conditions shown in Figure 10 are nearly identical to those in Figure 8, except that the curves are now labeled with values of the polymer fragment diffusivity, around  $10^{-11} \text{m}^2/\text{s}$ , that bring the calculations into agreement with the measured data. These diffusivities are about 100 fold smaller than those of metal ion species in plating baths. Although we do not have reliable estimates of polymer fragment diffusivities, they are expected to be very small owing to their large sizes and molecular weights. The data presented by Zanghellini et al.<sup>3</sup> for dip development rates can be used to estimate the product of the diffusivity and the polymer fragment concentration at the development surface. Based on this product and a diffusivity of  $10^{-11} \text{m}^2/\text{s}$ , the polymer fragments would represent about 10% of the bulk fluid density at the feature bottom, a reasonable outcome. Better estimates of polymer fragment diffusivity are certainly needed.

Zanghellini et al.<sup>3</sup> also report development rates for features ranging from 30-300  $\mu\text{m}$  in a bath having an acoustic intensity of 2  $\text{watts}/\text{cm}^2$ , five times less than that used in the experiments shown in Figure 10. Since the Peclet number would then be five times smaller than before, Figure 9 suggests that there would be very little acoustic enhancement in the 30 $\mu\text{m}$  features, but that wider features may still be enhanced. The data appear to show this trend for smaller feature depths, though the variation diminishes as depths grow larger. Similar data is reported by El-Kholi, Mohr, and Stransky.<sup>6</sup> We will be undertaking further analysis of these data sets.

Other experimental studies appear less relevant to LIGA. In particular, a number of studies have explored acoustic enhancement of development in features having widths of 10-50 nm using bath frequencies around 40 kHz<sup>6,7</sup>. Since these feature widths are far too small to accommodate acoustic streaming, it seems likely that bubble collapse is the operative mechanism, particularly since feature depths are only on the order of 100 nm. These bubble collapse phenomena will not provide the same benefit on the larger feature scales of interest in LIGA where, again, acoustic streaming is expected to occur.

## 7. SUMMARY

Although acoustic agitation is known to increase LIGA development rates, the physical mechanism of this enhancement has not been previously explained. The collapse of acoustic bubbles may play a role in removing polymer fragments from the developing surface, thereby increasing development rates in shallow features. However, bubble collapse does not readily explain enhanced development in deep, high aspect-ratio features in which development rates are limited by fragment transport along the feature.

The thesis of this paper is that high-frequency sonic agitation enhances development by producing a steady acoustic streaming flow that circulates most of the fluid within high aspect-ratio features, substantially increasing polymer fragment transport. In support of this hypothesis, analytical and numerical methods have been used to solve the equations governing flow and transport induced by acoustic agitation within trench-like LIGA features. Exact solutions derived by Rayleigh<sup>9</sup> were used to represent the acoustic wave fields within features, including the viscous boundary layers adjacent to feature walls. Since the acoustic boundary layer thickness is only about 1 micron for an agitation frequency of 1MHz, wave attenuation is negligible along features up to 1 millimeter in depth provided that the feature width is at least several microns.

Reynolds stresses produced by the high frequency motion induce a steady streaming motion downward along the feature walls at speeds on the order of 25  $\mu\text{m}/\text{s}$ . This downward flow is balanced by an upward flow of comparable speed along the feature center. The resulting bi-directional flow along the midsection of deep features was described using analytical solutions of the one-dimensional Stokes flow equations. For LIGA features wider than 20-30 microns the maximum downward velocity is determined mainly by shear forces within the acoustic boundary layers, not by shear forces on the interior side of the velocity maximum. Under these conditions the steady flow within the feature moves as though it were driven by a downward slip velocity along the feature wall and the slip speed is nearly independent of the feature width.

Polymer fragment transport along typical LIGA features was computed by numerically solving the Navier-Stokes equations together with a species transport equation accounting for fragment diffusion and advection. It was found that the four-fold enhancement in development rates observed by Zanghellini et al.<sup>3</sup> is consistent with model calculations based on a diffusivity of about  $10^{-11} \text{m}^2/\text{s}$ , a reasonable value for large polymer fragments. The acoustic streaming model further suggests a relatively weak variation of development rate with aspect ratio, in agreement with the Zanghellini data. It is also predicted that for Peclet numbers of 50 or more, development rates will increase about linearly with the acoustic intensity of the bath and with feature size.

It is concluded that acoustic streaming is probably the operative mechanism of acoustic enhancement in development of high aspect-ratio LIGA features. This mechanism is not, however, operative at the much smaller submicron scales typical of some microelectronics applications.<sup>6,7</sup> Nor is it beneficial in LIGA electroplating because there the metal ion diffusivity is sufficiently large that diffusive transport greatly exceeds transport by acoustic streaming.

The results reported here are based on a fundamental, though highly idealized, model of transport by acoustic streaming. Further work is required to explore acoustic coupling of the bath to the feature and the role of wave reflections from the feature bottom. Additional data is also needed to support model validation. The ultimate goal of this work is the use of physically-based models for LIGA process and hardware optimization.

## 8. ACKNOWLEDGMENT

This work was supported in part by the Sandia Materials Science Research Foundation and in part by the Sandia Accelerated Strategic Computing Initiative. Sandia is a multiprogram laboratory operated by Sandia Corporation, a Lockheed Martin Company, for the United States Department of Energy under contract DE-AC04-94AL85000.

## 9. REFERENCES

1. E. W. Becker, W. Ehrfeld, P. Hagmann, A. Maner, D. Munchmeyer, "Fabrication of Microstructures with High Aspect Ratios and Great Structural Heights by Synchrotron Radiation Lithography, Galvanofarming and Plastic Moulding (LIGA Process)," *Microelectronic Eng.* **4**, pp. 35-56, 1986.
2. D. Munchmeyer and W. Ehrfeld, "Accuracy Limits and Potential Applications of the LIGA Technique in Integrated Optics," Proceedings of the SPIE, *Micromachining of Elements with Optical and other Submicrometer Dimensional and Surface Specification* **803**, pp. 72-79, 1987.
3. J. Zanghellini, S. Achenbach, A. El-Kholi, J. Mohr, and F. J. Pantenburg, "New Development Strategies for High Aspect Ratio Microstructures," *Microsystem Technologies* **4**, pp. 94-97, 1998.
4. S. K. Griffiths, R. H. Nilson, R. W. Bradshaw, A. Ting, W. D. Bonivert, J. T. Hachman and J. M. Hruby, "Transport Limitations in Electrodeposition for LIGA Microdevice Fabrication", Proceedings of the SPIE, *Micromachining and Microfabrication Process Technology IV* **3511**, pp. 364-375, 1998.
5. A. El-Kholi, J. Mohr, and R. Stransky, "Ultrasonic Supported Development of Irradiated Microstructures," *Microelectronic Engineering* **23**, pp. 219-222, 1994.
6. K. J. Lee, J. Bucchignano, J. Gelorme, and R. Viswanathan, "Ultrasonic and Dip Resist Development Processes for 50 nm Device Fabrication," *J. Vac. Sci. Technol.* **B 15** (6), pp. 2621-2626, 1997.
7. T. Iwamoto, H. Shimada, S. Shimomura, M. Onodera, and T. Ohmi, "High Reliability Lithography Performed by Ultrasonic and Surfactant-Added Developing System," *Jpn. J. Appl. Phys.* **33**, Pt. 1, No. 1B, pp. 491-495, 1994.
8. T. G. Leighton, *The Acoustic Bubble*, Academic Press, London, 1994.
9. J. W. S. Rayleigh, *The Theory of Sound*, Dover, New York, 1945.
10. W. L. Nyborg, "Acoustic Streaming," Chapter 7 of *Nonlinear Acoustics*, M. F. Hamilton and D. T. Blackstock, eds., Academic Press, London, 1998.
11. J. Lighthill, "Acoustic Streaming," *Journal of Sound and Vibration* **61** (3), pp. 391-418, 1978.
12. K. Naugolnykh and L. Ostrovsky, *Nonlinear Wave Processes in Acoustics*, Cambridge University Press, Cambridge, 1998.